

KEPLER PLANETS: A TALE OF EVAPORATION

JAMES E. OWEN

Canadian Institute for Theoretical Astrophysics, 60 St. George St., Toronto, M5S 3H8, Canada

AND

YANQIN WU

Department of Astronomy and Astrophysics, University of Toronto, ON M5S 3H4, Canada

Draft version November 1, 2018

ABSTRACT

Inspired by the *Kepler* mission's planet discoveries, we consider the thermal contraction of planets close to their parent star, under the influence of evaporation. The mass-loss rates are based on hydrodynamic models of evaporation that include both X-ray and EUV irradiation. We find that only low-mass planets with hydrogen envelopes are significantly affected by evaporation, with evaporation being able to remove massive hydrogen envelopes inward of ~ 0.1 AU for Neptune-mass objects, while being negligible for Jupiter-mass objects. Moreover, most of the evaporation occurs in the first 100 Myr of the star's lives when it is more chromospherically active. We construct a theoretical population of planets with varying core masses, envelope masses, orbital separations, and stellar spectral types, and compare these against the sizes and densities measured for low-mass planets, both in the *Kepler* mission and from radial velocity surveys. This exercise leads us to conclude that evaporation is the driving force of evolution for close-in *Kepler* planets. In fact, some 50% of the *Kepler* planet candidates may have been significantly eroded. Evaporation explains two striking correlations observed in these objects: a lack of large radius/low density planets close to the stars, and a possible bimodal distribution in planet sizes with a deficit of planets around $2R_{\oplus}$. Planets that have experienced high X-ray exposures are generally smaller than this size, and those with lower X-ray exposures are typically larger. A bimodal planet size distribution is naturally predicted by evaporation model, where, depending on their X-ray exposure, close-in planets can either hold on to hydrogen envelopes ~ 0.5 -1% in mass, or be stripped entirely. To quantitatively reproduce the observed features, we argue that not only do low-mass *Kepler* planets need to be made of rocky cores overlaid with hydrogen envelopes, but few of them should have initial masses above $20M_{\oplus}$, and the majority of them should have core masses of a few Earth masses.

Subject headings: planets and satellites: composition, formation, interiors, physical evolution

1. INTRODUCTION

The spectacular success of the *Kepler* mission has yielded thousands of planetary candidates (e.g. Borucki et al. 2011; Batalha et al. 2013). Most of these exoplanets are smaller than Neptune ($4R_{\oplus}$) and are likely to have masses between a few, to tens of earth masses. We can now hope to make substantial progress in understanding the origin and evolution of planetary systems by studying the interior composition and orbital structure of these objects.

However, well-known degeneracies prevents us from resolving their interior composition. A typical *Kepler* planet is likely composed of a dense core and a tenuous envelope: the core can be volatile-rich, rock-rich or iron-rich; the envelope can consist of steam or hydrogen/helium. Unlike the case of main-sequence stars, radius measurement of these systems (all that is possible for most *Kepler* candidates) can not be used to constrain their structure. Even in the case where planetary masses are measured (via transit-timing-variations, TTV, or radial velocity, RV), multiple solutions for the interior structure exist. For instance, a Neptune-massed planet, with a density of 2 g cm^{-3} , can have either a thin hydro-

gen/helium envelope surrounding a dense rocky core, or be entirely ice/water dominated (e.g. Adams et al. 2008; Rogers & Seager 2010).

But this degeneracy can be broken by studying a population of planets and investigating how planetary sizes and densities correlate with their physical environment (Wu & Lithwick 2013). In particular, for those planets at close separations from their parent star (<0.2 AU), the total received high energy irradiation over Gyr time-scales can represent a considerable fraction of their gravitational binding-energy (e.g. Lammer et al. 2003; Lecavelier des Etangs 2007; Davis & Wheatley 2009). If these planets have hydrogen-rich envelopes, evaporation of these envelopes could markedly reduce their sizes and increase their bulk densities, when compared to planets further out.

Two recent studies have looked for correlations with separation. Ciardi et al. (2013) note that, for pairs of *Kepler* planets that are bigger than Neptune ($4R_{\oplus}$, these almost certainly have hydrogen envelopes), the inner planets are more frequently the smaller ones. However, they do not observe such a hierarchy in pairs smaller than Neptune. Therefore, they concluded that the correlations may be a result of the planet formation process, as opposed to any post-formation process. This conclusion contrasts with that arrived by Wu & Lithwick

(2013); in this study, they measure planetary masses in a sample of TTV pairs and find that, within pairs, the inner planets tend to be denser. Moreover, when considering all available mass measurements together, they find that planet densities increase with decreasing orbital periods. Therefore, they conclude that the low-mass planets observed by *Kepler* are composed of dense rocky cores overlaid with various amounts of hydrogen in their envelopes, which are then sculpted by evaporation. The same density and radius trends are encapsulated in many of the *Kepler* multi-planet systems, e.g., Kepler-11 (Lissauer et al. 2011), Kepler-18 (Cochran et al. 2011), Kepler-20 (Gautier et al. 2012) & Kepler-36 (Carter et al. 2012), as well as reported by recent radial velocity studies (Weiss et al. 2013). Thus an important question has arisen: are the observed correlations (radius/density vs. distance) results of formation or evaporation?

On the theoretical side, there is a large body of literature discussing planet evaporation, ever since the first hot Jupiters were discovered (e.g. Lammer et al. 2003; Yelle 2004; Tian et al. 2005; Hubbard et al. 2007a,b; Murray-Clay et al. 2009; Koskinen et al. 2010; Owen & Jackson 2012). Most of these deal with gas-giants, and only a few focus specifically on low-mass planets. We summarize two works here that are of direct relevance to our discussion.

Owen & Jackson (2012) develop realistic models of hydrodynamic evaporation for low-mass planets, including both X-ray and EUV irradiation. They perform the calculations on planet models of different densities and radii. They identify that only low mass-planets ($M_p < 60 M_\oplus$) could experience a significant effect from evaporation and suggest that evaporation may lead to a stability boundary below which all observed planets should lie (e.g. Koskinen et al. 2007). Lacking a thermal evolution model, they could not make predictions on final planet radius and density. The detailed evaporation models allow Owen & Jackson (2012) to calibrate the evaporation efficiency and they argue that this parameter can vary by orders of magnitude over the stellar and planetary lifetimes. Their work also highlight the relative importances of X-ray versus EUV evaporation.

Lopez et al. (2012) provide the only significant attempt to study the combined effects of thermal evolution and evaporation. Adopting a simplified energy-limited formalism for evaporation and a constant efficiency factor -the caveats of which are discussed in Section 2- and they also infer the presence of an evaporation threshold. They find that since the evaporation time-scale scales with planet mass \times planet density, that planets with mass \times density above a critical value would be evaporated above it. But as is demonstrated by Owen & Jackson (2012), a simplistic evaporation model may severely over- or under-estimate the mass-loss rates, especially in the first stages of the stars' and planets' lives.

Now with the large *Kepler* data set, evaporation of low-mass planets deserves a better study and a direct comparison with the observations. Moreover, it is useful to be able to predict the final planet size and density, for a given initial model. This allows us to backtrack the original planetary structures at formation. To accomplish these goals, we need to improve on previous work, in particular, we need to couple realistic calculations of evaporation with thermal evolution models.

We describe our approach in Section 3, after briefly reviewing the evaporation theory in Section 2. We then compare our theoretical results directly against observations in Section 4. Our evaporation theory successfully explains a number of observed facts, establishing that evaporation is the driving process of evolution for close-in *Kepler* planets. In fact, some 50% of the currently known *Kepler* planets may have been significantly affected by evaporation. Finally, we discuss the caveat and implications of our work in Section 5 and conclude in Section 6.

2. PHYSICS OF PLANETARY EVAPORATION

Planet evaporation can take place through a variety of mechanisms: non-thermal escape; thermal Jean's escape and hydrodynamic escape. Hydrodynamic evaporation occurs when the density of the heated region is sufficiently high so that the gas is collisional even in the super-sonic region of the flow. Thus, it is only hydrodynamic evaporation that can produce high enough mass-loss to affect the structure and sculpt the planet, which occurs at high incident fluxes; we focus on this mechanism.

As high-energy photons from the star ionize gas in the upper envelope (either hydrogen or metals), the newly freed electrons heat up the local gas and the atmosphere expands. A flow may be initiated that eventually escapes from the gravitational well of the planet. Let the efficiency of converting received energy to PdV work be η , so the mass-loss rate is simply:

$$\dot{M} = \eta \frac{L_{\text{HE}} R_p^3}{4GM_p a^2} \quad (1)$$

where L_{HE} is the high energy luminosity (X-rays or EUV), M_p is the planet mass, R_p is the planet radius and a is the separation from the parent star.

The usual so-called 'energy-limited' approach is equivalent of taking η to be an order-unity constant (e.g. Watson et al. 1981; Lammer et al. 2003; Lecavelier des Etangs 2007; Erkaev et al. 2007). Under such an assumption, the evaporative time-scale is $M_p/\dot{M} \propto M_p \rho / F_{\text{HE}}$, where F_{HE} is the high energy flux. So Equation 1 lends itself to an evaporation threshold in terms of mass \times density (Lopez et al. 2012).

However, the evaporation efficiency is not always constant but may vary significantly with planet mass, radius and the ionizing flux (see Section 5). Murray-Clay et al. (2009) demonstrated that, in the case of EUV evaporation of hot Jupiters, the 'energy limited' approximation is only valid at low fluxes. At high fluxes, the mass-loss process is controlled by the ionization/recombination balance, yielding mass-loss rates that scale as $L_{\text{EUV}}^{1/2}/a$, or, the 'efficiency' (η) decreases with flux. This limit (the 'recombination-dominated' regime) is similar to EUV driven evaporation of gas clumps (Bertoldi & McKee 1990) and protoplanetary discs (e.g. Johnstone et al. 1998; Hollenbach et al. 2000).

For X-ray ionization, Owen & Jackson (2012) showed similarly that the evaporation is not 'energy-limited', but rather the 'efficiency' is controlled by line cooling, and is a strong function of planet mass. They found that cooling is most important for high mass Jovian planets, since

the higher planet escape temperature and larger physical size mean flow time-scale is long. Then there is then much time to radiate away the received heating when the flow is still sub-sonic. For lower mass, Neptune-like planets, the escape velocity is much lower and the physical sizes smaller, meaning the flow time-scale is shorter, so much less energy is radiated away and the corresponding ‘efficiency’ (η) is higher. While Owen & Jackson (2012) found that the X-ray evaporation gives a similar flux-scaling as given in Equation 1, the flow is not close to being ‘energy-limited’ (where PdV work is the dominant energy loss channel), and only begins to approach an energy-limited case at low masses $< 3 M_{\oplus}$. Furthermore, Owen & Jackson (2012) noted that unlike the EUV case, since the X-ray driven mass-loss scaled as L_X/a^2 at high and low fluxes there is no transition from line-cooling limited to energy limited at low X-ray fluxes.

The ionizing flux from a main-sequence star varies by orders of magnitude through its life. In addition, the size of a planet also changes over time, under both thermal contraction and mass-loss, along with the mass of the planet decreasing. With η being a function of planet mass and radius, as well as the ionizing flux (see Figure 12), one should not adopt a constant η (as in Lopez et al. 2012) in tracing out the evaporation history of the planet. It is important that the correct prescription of evaporation is used to follow the planetary evolution, particularly for low mass planets where evaporation can significantly affect the evolution. This is essential if one wants to make inferences about the initial state of these planets.

The last issue worth attention is the nature of the ionizing flux. Which source of high energy luminosity is driving the evaporation has only been tackled recently. Some authors have purely used EUV flux in their studies (e.g. Lecavelier des Etangs 2007), while others have used only the X-rays (Jackson et al. 2012). Owen & Jackson (2012) solved the flow problem including both X-ray and EUV irradiation. They found that the position of the transition from sub-sonic to super-sonic flow (the ‘sonic point’), relative to the respective ionization fronts, determines whether X-rays or EUV is driving the mass-loss. At a similar ionizing energy flux, they found that X-ray drives the mass-loss when the flux is high, and EUV dominates the mass-loss when the flux is low. For the first ~ 100 Myrs of their lives, main-sequence stars have X-ray luminosities that reach up to $\sim 10^{-3}$ of their bolometric luminosities; this fraction falls off with time roughly as $1/t$ as the stars age (Güdel 2004; Ribas et al. 2005; Jackson et al. 2012).

3. EVOLUTIONARY MODELS OF PLANETARY EVAPORATION

In order to follow the evolution of a close-in planet, we need to include the effects of thermal cooling of the planet, irradiation of its upper atmosphere and mass-loss in the form of hydrodynamic evaporation. Previously, Lopez et al. (2012) have addressed this problem by coupling the Fortney et al. (2007b) and Nettelmann et al. (2011) planetary structure models to a simplistic energy-limited estimate for the mass-loss. We aim to achieve a similar goal here, but we will base our mass-loss rate on a realistic calculation that include both the X-ray and EUV radiation (Owen & Jackson 2012). We make use

of the MESA stellar evolution code (Paxton et al. 2011, 2013) to model the thermal evolution and couple it to the Owen & Jackson mass-loss calculations.

3.1. Method

The general purpose MESA code provides the framework to simulate planetary structure and evolution. Our planet models have solid inner cores, experience irradiation (under the two stream approximation, e.g. Guillot 2010), and evaporation. The MESA equations of state is discussed in detail in Paxton et al. (2011), but in the planetary regime is typically based on the SCVH equation of state (Saumon et al. 1995). The opacity tables are used for the irradiation of the atmosphere are based on an updated version of the Freedman et al. (2008), as detailed in Paxton et al. (2013), where we adopt an opacity $\kappa_* = 4 \times 10^{-3} \text{ cm}^2 \text{ g}^{-1}$ to the incoming stellar irradiation suitable for a solar type star (Guillot 2010).

To include evaporation, we tabulate the mass-loss rates as functions of ionizing flux, planet mass and planet radius, using the results in Owen & Jackson (2012). The tabulated results span a range in planet mass from $1M_{\oplus}$ to $3M_J$, and in planet radius from $1R_{\oplus}$ to ~ 0.01 AU (roughly the Hill radius at 0.1 AU for our most massive planet). For the ionizing X-ray flux, we adopt the observed relation between this flux and stellar spectral type and stellar age (Jackson et al. 2012). In general, the X-ray luminosity saturates at $\sim 10^{-3}$ of the stellar bolometric luminosity during the first ~ 100 Myrs of the star’s life, and decays approximately as $1/t$ afterwards. Furthermore, following Owen & Jackson (2012), we take the EUV luminosity to follow the same time evolution of the X-rays.

Since convective transport is the dominant heat transport mechanism in the planet’s envelope, the thermal structure of the envelope is set to be initially adiabatic, in the absence of irradiation. The radius of the planet is defined to be at a radius where the optical depth to the incoming bolometric radiation is $2/3$, and is typically around milliBar (for younger and lower mass planets) to Bar (for older and more massive planets) pressures for the planets considered here. This planet radius is also taken as the input radius in the evaporation model. Since the atmosphere’s underlying scale height is typically small compared to the planet radius, such an approximation is accurate. For the same reason, we have ignored the difference between the above radius and the radius a planet exhibits at transit (Hubbard et al. 2001). But such a simplification may break down for the closest in planets at the earliest times, where there may be a $\sim 10\%$ difference in a planet’s optical photosphere and the base of the evaporative flow. However, given that planets quickly contract through such a phase, the effect will be negligible when integrated over the Gyrs of planetary evolution.

Our planets are composed of two separate regions: an envelope of Hydrogen/Helium with a metallicity at solar abundances (as used for the evaporation models), and a solid core. Given the large range of possible core compositions, as a starting point we focus on a pure rock core, using the mass-radius profile provided by Fortney et al. (2007a,b), with core masses (M_c) of 6.5, 7.5, 10, 12.5 & 15 M_{\oplus} adopted. These cores are assumed to of

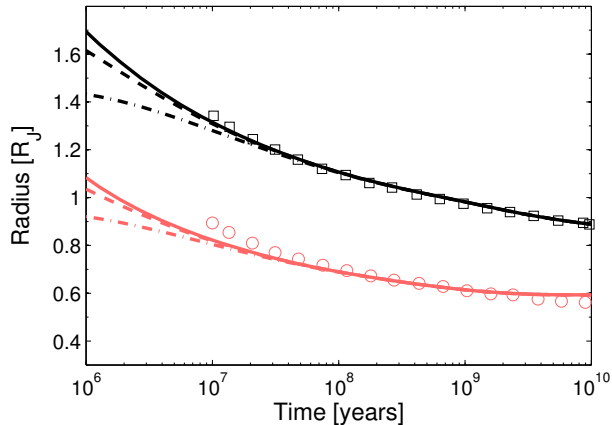


FIG. 1.— Benchmark calculations of our modified version of MESA against the calculations of Fortney & Nettelmann (2010) for 95 (squares) & 32 (circles) M_{\oplus} planets at a separation of 0.045 AU from a sun-like star. Our calculations are shown for three initial cooling times of 10^5 (solid line), 10^6 (dashed line) and 10^7 (dot-dashed line) years. Agreement is at the $\leq 5\%$ level in all cases.

fixed radius and do not evolve during the planets evolution. However, the cores do have a thermal content from from both radioactive decay and thermal heat capacity where we adopt an earth-like value (see Nettelmann et al. 2011, Lopez et al. 2012). Both of which are implemented in MESA using the core luminosity function (Paxton et al. 2013). As current planet formation models are unable to provide a good handle on the initial thermal properties of formed planets (e.g. ‘hot’ or ‘cold’ start) we consider initial models with a wide range of initial radii. This initial radii (or more correctly entropy) is parametrised in terms of an initial cooling time (t_{cool}), which we define as the ratio of a planet’s initial internal energy to a planet’s initial luminosity. We could of course parametrise the initial entropy in terms of some other variables; however, the initial cooling time is perhaps the most interesting as this be compared to protoplanetary discs lifetimes ~ 3 Myr (e.g. Haisch et al. 2001; Hernández et al. 2007; Owen et al. 2011; Armitage 2011).

In order to make sure our model is following the evolution of low-mass planets accurately we benchmark our calculations against the models presented in Fortney & Nettelmann (2010 - their Figure 10); the calculations were performed using the Fortney et al. (2007a) code for a 95 & 32 M_{\oplus} planet with a 25 M_{\oplus} core¹ that is a 50/50 mix (by mass) of ice and rock. We follow the evolution of these planets under the influence of irradiation by a sun-like star, but no evaporation. We find excellent agreement to these calculations at the $\leq 5\%$ level giving confidence our modified version of MESA is performing as expected at low-masses. In Figure 1 we show the radius evolution of our calculations for cooling times of 10^5 (solid line), 10^6 (dashed line) and 10^7 (dot-dashed line) years. These calculations are compared against the results from the Fortney & Nettelmann (2010) at a separation of 0.045AU shown as points for both the 95 (squares) & 32 (circles) M_{\oplus} planets.

For our calculations we choose values of t_{cool} (com-

¹ We note the Fortney et al. (2007) calculations used a core with no thermal contribution and we do the same for the benchmark calculations.

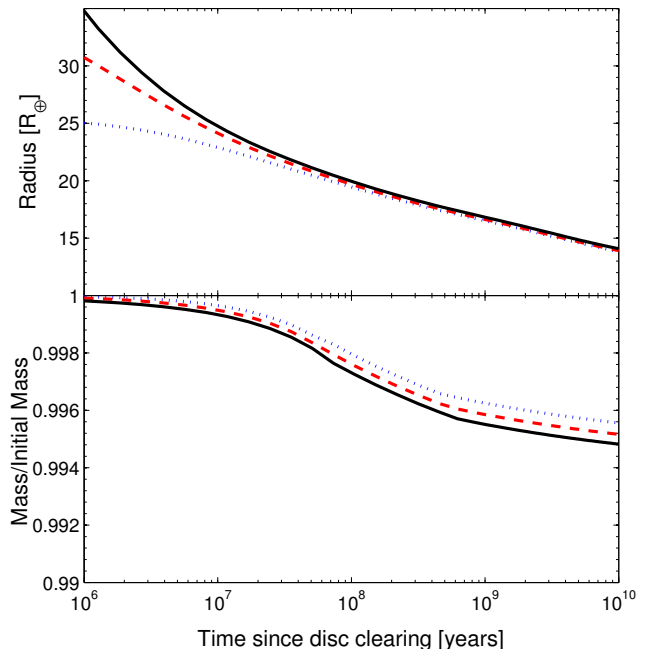


FIG. 2.— The top panel shows the radius evolution of Jupiter like planets as a function of time since gas disc clearing, at a very close separation to their parent star (~ 0.025 AU); the bottom panel shows the mass evolution of this planet. The solid line represents a planet with an initially high entropy with an initial cooling time of 10^6 years, the dashed line has an initial cooling time of 10^7 years, and the dotted line has an initially low entropy with an initial cooling time of 10^8 years.

puted in the absence of irradiation) in the range $3 \times 10^6 - 10^8$ years to span a range of ‘hot’ start and ‘cold’ start model, similar to those values chosen by Lopez et al. (2012). We note that with cooling times $< 3 \times 10^6$ years most low mass planets at separations < 0.1 AU have initial radii larger than their Hill radii, and they cannot be considered hydrostatically bound objects.

For each cooling time and each core mass, we construct 40 models with a range of envelope masses from 3 M_J to a few percent of the core mass, logarithmically spaced in envelope mass. The planets are then evolved forward in time, under the influence of evaporation and irradiation for 10 Gyrs or until the entire envelope is lost². Our integrations begin at 3 Myrs, a time at which the protoplanetary disc clears and the planet is fully exposed to the X-ray and EUV irradiation. In general the planets evaporation begins in the X-ray driven phase, and may switch to EUV driven at some late time. Where the planets’ final mass is set by a few 100 Myrs.

3.2. Jupiter-like planets

Jupiter mass planets close to their central stars represent the case where there is direct observational evidence (e.g. Vidal-Madjar et al. 2003, 2004) of evaporation occurring. Thus, it is worth investigating whether there are any evolutionary consequences for the evaporation of high-mass planets. For example, Baraffe et al. (2004) noted that if the evaporation rate was high enough, so

² Thus, we ignore any subsequent mass-loss from the core due to sublimation, which may happen at the highest equilibrium temperatures $T_{\text{eq}} \gtrsim 2000$ K (e.g. Perez-Becker & Chiang 2013).

that the evaporation time ($\sim M_p/\dot{M}$) became comparable to the thermal time of the planet’s envelope, then a Jupiter mass planet could lose its entire envelope rapidly. Such an inference was based upon the rather unrealistic assumption of 100% mass-loss efficiency. In reality, at high masses the mass-loss rates never reach such high values (see Owen & Jackson 2012 for a more detailed discussion). To illustrate this we show the evolution of a Jupiter-like planet at a very close separation of 0.025 AU around a solar type star in Figure 2. We plot the radius and mass evolution of planets with a $15M_{\oplus}$ rock core and cooling times ranging from the very short (10^6 years - solid) to the very long (10^8 years- dotted). Figure 2 clearly shows that evaporation is unable to effect the planets’ evolution and planets with very different initial cooling times end up on almost identical evolutionary tracks at late times. With the mass-change in the planets at the $< 1\%$ level, as argued for by Hubbard et al. (2007a).

Therefore, while Jupiter mass planets currently provided the best opportunity for actually studying the hydrodynamics of evaporation by directly probing the flow, they do not provide a good laboratory for studying the evolutionary consequences of evaporation and we must go towards lower mass planets where the evolutionary effect will be more pronounced.

3.3. Low-mass planets

Unlike the Jupiter-type planets discussed above, several authors have suggested that the effects of evaporation will be more prominent around lower mass planets (e.g. Hubbard et al. 2007a; Baraffe et al. 2008; Jackson et al. 2012; Owen & Jackson 2012; Lopez et al. 2012). At lower masses evaporation can begin to sculpt the planet population, removing significant amounts of a planet’s envelope during its lifetime. To investigate this we show the evolution of a low mass planet in Figure 3, where we consider the evolution of a ‘standard’ model which is an initially $20 M_{\oplus}$ planet with a $12.5 M_{\oplus}$ core. Figure 3 shows the evolution of the ‘standard’ model for the full range of initial cooling times considered. The planets are at a close separation of ~ 0.05 AU and have equilibrium temperatures of 1300K. Where we define the equilibrium temperature as the black body temperature at a given separation, i.e.:

$$T_{\text{eq}} = T_* \sqrt{\frac{R_*}{2a}}, \quad (2)$$

where T_* and R_* are the parent star’s temperature and radius respectfully.

The panels in Figure 3 show the qualitative features of the evolution of low-mass planets. In particular, planets with higher initial entropies have initially larger radii and therefore lose more mass. The result is that planets with shorter initial cooling times end up with, smaller radii and higher densities than planets with longer initial cooling times. At low masses evaporation plays a strong role in planetary evolution, which in the case of our ‘standard’ model makes the planets a factor of ~ 2 smaller and a factor of ~ 4 denser compared to the same planet that is not undergoing evaporation. In this case an initial envelope containing $\sim 40\%$ of the original mass is evaporated down to one containing only few percent of the total mass, and in the most extreme case (for the

planet with an initial cooling time of 3×10^6 years) evaporation leaves a planet with 0.5% of the total mass in a Hydrogen/Helium envelope.

The bottom, right-hand panel of Figure 3 shows the evolution of $\dot{M} \times \text{age}$, which indicates when the mass-loss is most significant. This plot shows that in all cases the mass-loss is most important at roughly the point where the X-ray luminosity begins to decline. This is easy to understand as at early times the planets are large and the fluxes are high, so the planet can absorb a significant amount of high energy radiation. Once the X-rays begin to decline the planet evolution is affected less by evaporation and once the evaporation switches to EUV driven the final planet properties have already been ‘frozen’ in, similar to the results from the previous models calculated by Owen & Jackson (2012) and Lopez et al. (2012). This is a rather generic feature of all the evolutionary models, where the saturation time-scale for the X-rays sets the length of time which evaporation is important in driving the planets’ evolution, and that there is very little change in the planets’ mass from 100 Myrs to 10 Gyrs.

4. POPULATION STUDY AND COMPARISON AGAINST OBSERVATIONS

We have shown that, for low mass planets close to their parent star, a significant amount of the planet’s gaseous envelope, or even an entire atmosphere, can be removed in Gyr time-scales.³ Given the prominent role evaporation can play, we can use this evolution to make inferences about the initial structure of observed close-in planets, and provide clues as to their formation. In the following, we provide comparisons between our theoretical models and observations, mostly using data from the *Kepler* mission. The effects of evaporation are clearly visible in data. In fact, the evaporation model naturally explains a number of remarkable correlations seen in the *Kepler* data.

In Figure 4, we plot the final planet mass and radius as a function of separation for planets with initial properties which vary from our ‘standard’ model, where central star has $1 M_{\odot}$ in all cases. At a given planet mass, a lower core mass results in initially larger planets, which means that the planet can absorb a larger fraction of the X-ray flux, driving stronger evaporative flows. So planets with smaller cores may lose the entire envelope at a larger separations than those with larger cores (see Figure 8). The initial cooling time shows the same effect as discussed above, with shorter cooling times resulting in more mass-loss due to the initially larger radii; however, this effect is much less important than the effect of initial core mass. Finally, evaporation can drive convergent evolution. For instance, planets at $< 0.05 AU$ that had initial $15 M_{\oplus}$ cores, but envelopes of 2 & 5 M_{\oplus} end with somewhat identical structures. This means that, at least in some cases, it may be difficult to retrieve the planets’ initial structure, particularly at low envelope mass-fractions.

4.1. Upper Envelope in Planet Radius

³ We ignore all Jovian planets from now on. When comparing against Kepler data, this is naturally achieved by only plotting planets in multiple systems.

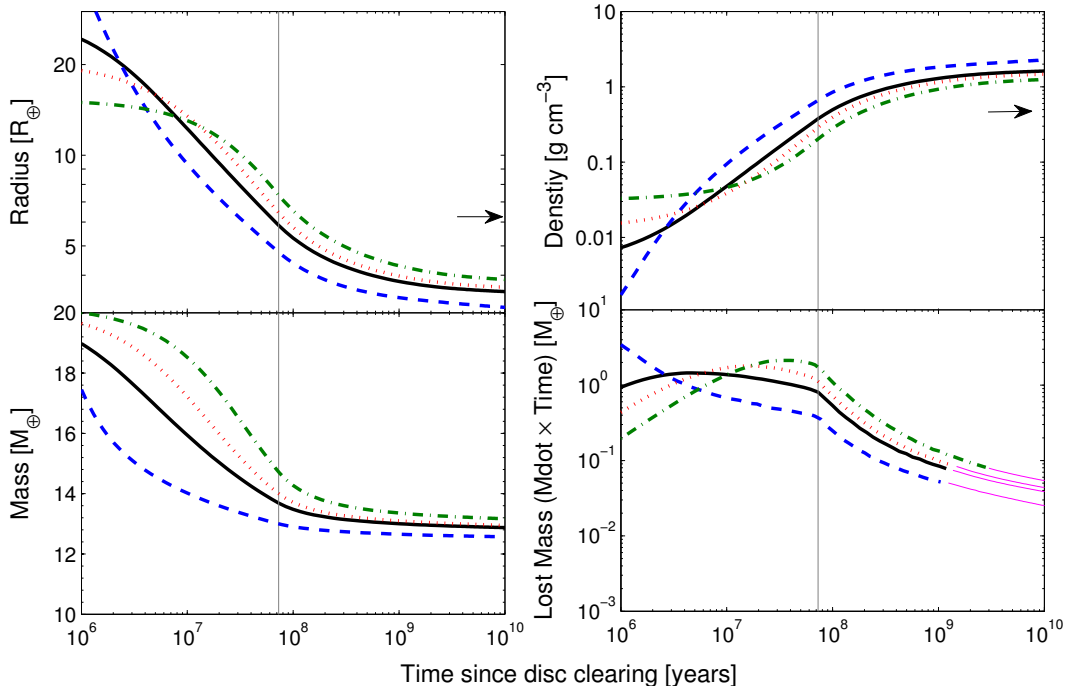


FIG. 3.— The evolution of a $20 M_{\oplus}$ planet with a $12.5 M_{\oplus}$ core at a separation of 0.05 AU is plotted, with four initial cooling times: 3×10^6 years (dashed); 1×10^7 years (solid); 3×10^7 years (dotted); 1×10^8 years (dot-dashed). In the upper left we show the radius evolution, the density evolution is shown in the upper right, the mass evolution in the bottom left and in the bottom right we show the time evolution of $\dot{M} \times \text{age}$ which indicates the times at which most mass-loss is occurring, with the thin continuation to these lines show the point at which the evaporation switches from X-ray driven to EUV driven. The final properties of the same planet not undergoing evaporation are shown by the small arrows.

The *Kepler* transiting-planet catalogue is the most extensive catalogue of planets on close orbits to their parent star; for better statistics, we use the *Kepler* object of interest (KOI) catalogue, which lists the radii (not mass) of planet candidates. Most of the KOIs have not been confirmed as planets, and there is a certain, but low, percentage of false positives (Morton & Johnson 2011). To minimize contamination, we choose to consider only KOIs that have been identified as being in multiple systems, where the significance of planetary nature is considerably higher ($\gtrsim 95\%$ Lissauer et al. 2012). The use of only multi-planet systems, while the most robust, may introduce some implicit biases. In particular, planets that may have been dynamically moved to small orbital periods at late times, will have undergone a different evolutionary path. Since we are interested in the long term evolution of planets due to evaporation, then the multi-planets KOIs represents the cleanest sample to begin with.

Plotting planet radius against separation for planets in multi-planet systems around solar-type stars ($T_* = 5200 - 6200$ K) we notice an upper-envelope in planet size that rises with separation. This has also been noticed by Ciardi et al. (2013) and Wu & Lithwick (2013). The lack of large planets at small separations is statistically significant: we cut the sample into 4 regions: large and small planets with a division at $R_p = 5 R_{\oplus}$ and hot and cold planets with a division at $T_{\text{eq}} = 1000\text{K}$, then comparing the ratio of large cold planets to the ratio of small cold planets. Where one would expect to observe ~ 20 hot large planets if these are the same populations, we find only 3.

We also argue that selection effect in the *Kepler* pipeline would not produce such an upper envelope. KOI candidates have to have a certain signal to noise ratio to be identified. This favours detecting smaller planets closer to the stars, as they have produced a larger number of transits during the mission lifetime. The completeness radius (sizes above which the KOI catalogue is complete) will rise with planet periods, similar to the upper envelope discussed here. We draw such a curve for the sub-sample considered by (Petigura et al. 2013) in Figure 5, which lies far below the upper envelope. Though more noisy stars than those considered by (Petigura et al. 2013) will move this curve upward, it will not explain the upper envelope.

This upper envelope is naturally explained by evaporation: low density planets can not survive in the environment of high ionizing flux. Quantitatively, evaporation of $20M_{\oplus}$ planets with rocky cores of masses $10-15 M_{\oplus}$ provides a good fit to the upper envelope, as is shown in Figure 5.

There is another implication to this agreement. If there were a significant population of planets with initial masses higher than, say, $30M_{\oplus}$ (dotted line in Figure 5), we would not expect to observe the same upper envelope. These more massive planets can hold on to their atmospheres, much like the hot Jupiters can (see Section 3.2), and would populate the upper left region in Figure 5. The absence of these more massive planets is interesting: perhaps not coincidentally, as $20 - 30 M_{\oplus}$ roughly corresponds to gap-opening mass in this region, suggesting that there is ceiling to how much gas the planets can accrete in this neighbourhood. The core

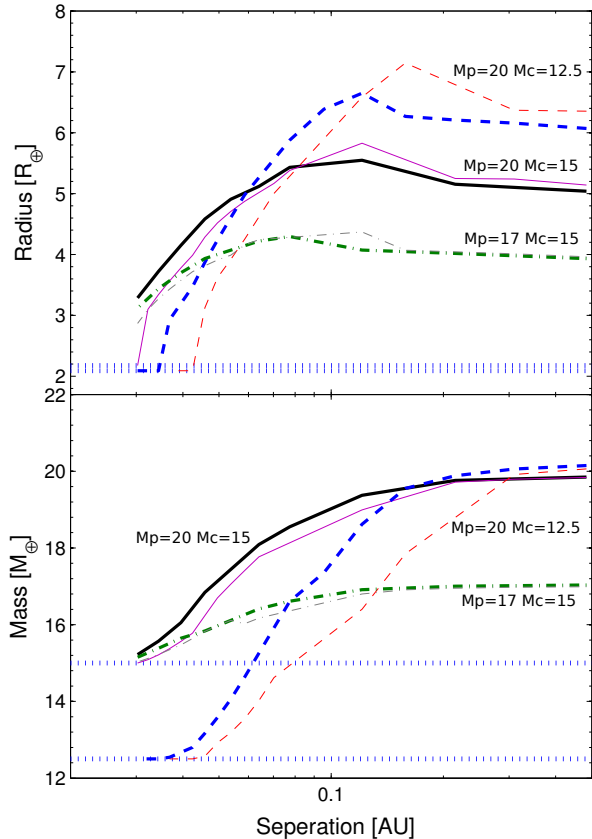


FIG. 4.— Final planet radius (top panel) and mass (top panel) as a function of separation, for models with different initial core mass (labelled as M_c), total mass (labelled as M_p) and initial cooling time (thin lines for 3×10^6 yrs and thick lines for 10^8 yrs, longer cooling time indicates lower internal entropy). The central star is sun-like. The straight dotted lines show the masses and radii of the rocky cores alone. Planets inward of ~ 0.1 AU experience significant mass-loss and can retain only a fraction of their primordial atmospheres (depending on the core mass), with the hottest ones exposed to bare cores. As a result, the maximum radii of these planets decrease inward.

mass also somewhat affects the upper envelope. We find that models with roughly half of the total mass in the rocky cores best reproduce the data, consistent with the conclusion in Wu & Lithwick (2013). In contrast, the planet’s initial cooling time makes little difference to the results.

4.1.1. Dependence on Stellar Spectral Types

The mass of the parent star is an important consideration. The parent stars direct influences on the evaporation, through its gravity is small. However, the total received X-ray flux at a fixed bolometric flux (so fixed equilibrium temperature) can vary greatly, with late-type stars being significantly more X-ray luminous when integrated over Gyr time-scales (Güdel 2004; Güdel et al. 2007; Jackson et al. 2012). We demonstrate this by considering the evolution of the ‘standard’ planet discussed above ($M_p = 20 M_{\oplus}$, $M_c = 12.5 M_{\oplus}$), at a fixed equilibrium temperature (1300K) around a later-type ($0.5 M_{\odot}$) and earlier-type ($1.5 M_{\odot}$) star compared to a planet around a solar type star, all with initial cooling times of 10^7 years.

The evolution of these planets, is shown in Figure 6,

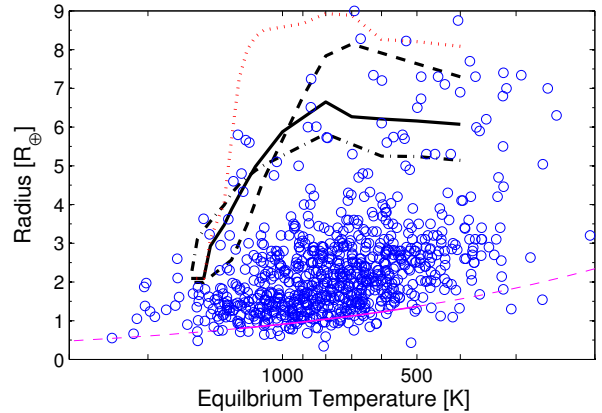


FIG. 5.— The upper envelope of planet sizes as a function of equilibrium temperature. The open circles show the Kepler Object of Interests that are around solar type stars ($T_{\star} = 5200 - 6200$ K) and are in multiple transiting systems. The black curves are the theoretical final radii for planet models with initial mass $20 M_{\oplus}$ and 10 (dashed), 12.5 (solid) & $15 M_{\oplus}$ (dot-dashed) of rocky cores. The dotted line are for $\sim 30 M_{\oplus}$ planets with $12.5 M_{\oplus}$ cores. All models here have an initial cooling time of 10^7 years. The thin line shows the 50% completeness limit calculated by Petigura et al. (2013) -solid- and extrapolated -dashed- to larger and smaller separations.

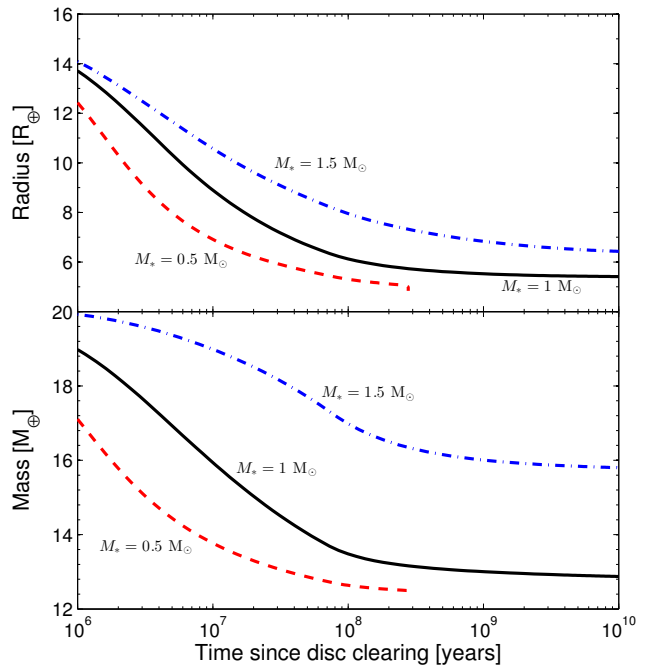


FIG. 6.— The panels show the radius (top panel) and mass (bottom panel) evolution of a planet ($20 M_{\oplus}$) with an equilibrium temperature of 1300K (~ 0.05 AU around a solar type star) and $12.5 M_{\oplus}$ rock core, around a $1.5 M_{\odot}$ star (dot-dashed), $1 M_{\odot}$ star (solid) & $0.5 M_{\odot}$ star (dashed). The solid lines are identical to the solid lines in Figure 3.

where the radius evolution is in the top panel and the mass evolution in the bottom panel.

Naively, one would expect a similar evolution as the bolometric flux revied is identical in all cases. However, the variation of X-ray luminosity with stellar mass results in qualitatively different evolutionary paths for the planets, with order-unity differences in both the final planet

mass and final planet radius. The planet around the $0.5 M_{\odot}$ star has had its envelope completely removed, whereas the planet around the $1.5 M_{\odot}$ planet still has a $\sim 3 M_{\oplus}$ envelope remaining after 10 Gyrs.

We can go further and compare our evaporation threshold found above for solar type stars to KOIs around other types of host stars. Lower mass stars (e.g., M-dwarfs) have higher X-ray flux, when compared to their bolometric luminosities. They also remain chromospherically active for longer periods. Figure 6 shows that, indeed, at the same equilibrium temperature (measuring the bolometric flux), the upper envelope around lower mass stars appear to be suppressed to smaller planet sizes.

Currently, the numbers of candidates around A/F and M stars are not as large as those around G/K stars. Thus, a fully quantitative comparison is not possible at this stage. Moreover, planet radii determination around M-stars suffer large uncertainties (Muirhead et al. 2012; Mann et al. 2012; Morton & Swift 2013), and radius determination for hot stars can also be polluted by the presence of sub-giants (Brown et al. 2011), and must bare this in mind when drawing inferences. We determine the theoretical evaporation threshold by extracting a linear relation between the maximum radii and equilibrium temperature, for planets with an initial mass of $20 M_{\oplus}$ and a core mass in the range $10 - 15 M_{\oplus}$, that are orbiting around a solar-type star and have equilibrium temperature in the range of $500 - 2000$ K. Since the total mass loss roughly scales linearly with the integrated X-ray flux, we expect the same radius threshold to apply to planets around all spectral types, when we arrange them by their X-ray exposure. This is shown in Figure 7, where the planets are separated by the spectral type of their parent star.⁴ In contrast, we show the same planet radii plotted against their bolometric exposure. Planets satisfy the same evaporation threshold only when one considers X-ray exposure. This argues that the ionizing flux, not the bolometric flux, is what determines the upper envelope. Furthermore, we also show the KOIs in single planet systems in Figure 7 as small filled circles, which show the same behaviour as the multi-planet KOIs, although with slightly more scatter.

4.2. Distribution of Radius

Our analysis in the previous sections suggest that the observed radius cut-off in KOIs is related to the fact that the most massive KOIs⁵ have masses not much exceeding $20 M_{\oplus}$ and that their core masses are roughly half of their total masses. Here, we investigate the nature of all KOIs by studying the overall radius distribution.

In Figure 8, we present the final radii of multiple sequences of planet models with initial cooling times in the range $3 \times 10^6 - 10^8$ years. These have core masses from $6.5 M_{\oplus}$ to $15 M_{\oplus}$, and atmosphere masses from approximately one percent of the core mass to much larger values. The total planet masses are restricted to $< 20 M_{\oplus}$. We do not consider atmospheres with masses below one percent, motivated by the discussion below. The radii are evaluated after 10 Gyrs of orbiting around a sun-like

⁴ Since the evolution of the X-ray luminosity is poorly known for stars $< 0.45 M_{\odot}$, we approximate the X-ray evolution of these stars with that of a $0.45 M_{\odot}$ star.

⁵ Aagain, we exclude Jovian planets from this discussion.

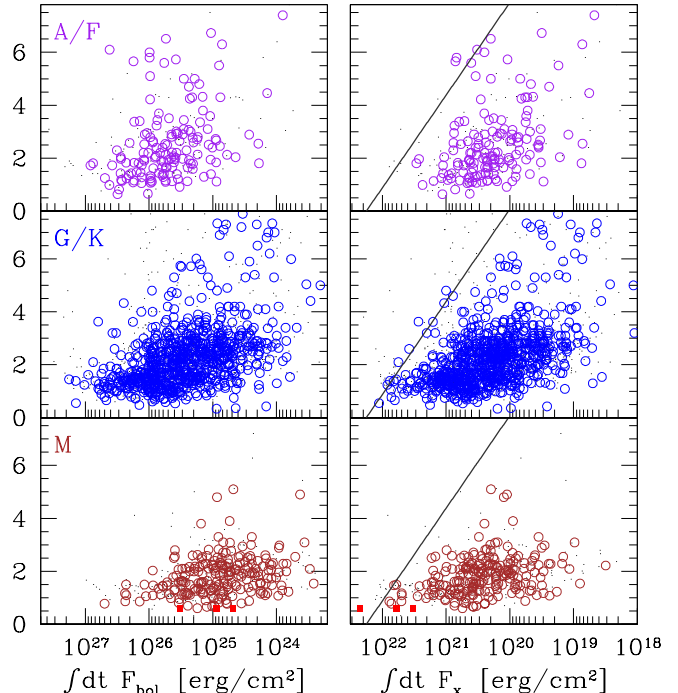


FIG. 7.— The observed radii of KOIs are plotted against their bolometric exposure (bolometric flux received at surface integrated over 10 Gyrs, left panels), and X-ray exposure (same but for X-ray exposure, using Jackson et al. 2012 values, right panels). The objects are roughly separated into those around A/F stars (top panels), G/K stars (middle-panels) and M-dwarfs (lower panels, the red squares stand for the system KOI 961). KOI multis are shown as open circles while KOI singles as small dots. As predicted by our models of x-ray evaporation, planets around stars of different spectral types, while having very different bolometric exposure, have roughly the same maximum sizes at a given x-ray exposure. The solid lines show the theoretical evaporation threshold derived from a linear fit to the black evaporation curves shown in Figure 5. The right panels demonstrate that planets around different types of stars satisfy the same maximum radius/X-ray exposure relation as that found around solar-type stars. One cannot perform the same exercise in the left panels.

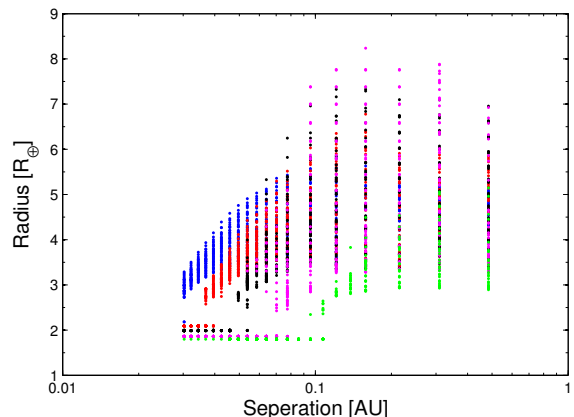


FIG. 8.— The final radii of planets with an initial mass $< 20 M_{\oplus}$, as a function of separation from a sun-like star. Different colours represent different core masses with blue standing for $15 M_{\oplus}$ core, red for $12.5 M_{\oplus}$ core, black $10 M_{\oplus}$, magenta $7.5 M_{\oplus}$ & green $6.5 M_{\oplus}$. We consider atmospheres as low in mass as one percent of the core mass. For all models, there is a critical separation within which the planets are evaporated down to bare cores. This separation is larger for models with smaller core masses.

star, though the values differ little if we instead evaluate at 1 Gyrs (e.g. Lopez et al. 2012; Lammer et al. 2013). Figure 10 shows the corresponding planet densities as a function of separation and is discussed in Section 4.3.

The overall population show the general feature noted previously, that the radius decreases with decreasing separation. One particularly interesting feature that appears is a gap in radius between planets that have gaseous envelopes, and those that are bare cores. For instance, for the $6.5 M_{\oplus}$ core models, inward of ~ 0.1 AU, all planets have their atmospheres stripped away with their final sizes reflecting that of their naked rocky cores; while outside ~ 0.1 AU, planets can retain atmospheres that are at least a fraction of a percent in mass, consequently they have sizes that are markedly larger. This bifurcation generates a gap in planet radius. The orbital separation at which this gap appears is smaller for planets that have bigger cores and stronger surface gravity. However, inside $\sim 0.03 AU$ there are no surviving planets with gaseous envelopes.

The origin for this gap is easy to understand. As planets lose their hydrogen atmosphere, they become increasingly compact and dense, which reduces the mass-loss rate. However, there is also less hydrogen to lose. So for planets inside the critical separation, the loss is total (e.g. Baraffe et al. 2006; Lopez et al. 2012). While for planets just outside the critical separation, there is a minimum atmosphere mass the planets need to avoid complete stripping. Any thinner atmosphere will be easily eroded. This mass is roughly 1% of the total mass and corresponds to roughly an order unity modification to the planet radius. So we expect to see a gap in planet size. Such a gap may become less pronounced when different core compositions are considered, but the basic property that small atmospheres are unstable to complete evaporation will always result in a region where planets are unlikely to end up. Observationally determining the presence of such a gap will place strong constraints on the model and further characterising the gap will allow useful inferences about the dominant core mass/composition.

In Figure 9, we demonstrate that the radius distribution of KOI multi-planet systems is suggestive of a bimodal distribution. Most planets have sizes $\sim 1.5R_{\oplus}$ or $2.5R_{\oplus}$, with a deficit of objects at radius $\sim 2R_{\oplus}$, indicative of the presence of a gap. To further test this suspicion, we divide the objects by their X-ray exposure into a high X-ray group (corresponding to < 0.1 AU around a solar-type star) and a low X-ray group. Strikingly, objects with a high X-ray exposure mostly have sizes below the gap, at $\sim 1.5R_{\oplus}$, while objects with a low X-ray exposure typically have sizes above the gap, at $\sim 2.5R_{\oplus}$. This argues that the deficit at $2R_{\oplus}$ could be physical and is associated with X-ray exposure.

The same bi-modal behaviour appears when we consider only KOI singles, both single and multi-planet KOIs, or when we include only bright KOI targets, or only dim KOI targets. In addition, the same behaviour is seen when we restrict ourselves to planets that have periods shorter than 50 days and sizes above $1.3R_{\oplus}$, a group of KOIs that suffer relatively little incompleteness effect (Petigura et al. 2013; Fressin et al. 2013). Although most careful studies to date have yet to have sufficient radius resolution to confirm this feature (Howard et al. 2012; Petigura et al. 2013; Fressin et al. 2013), it is hinted

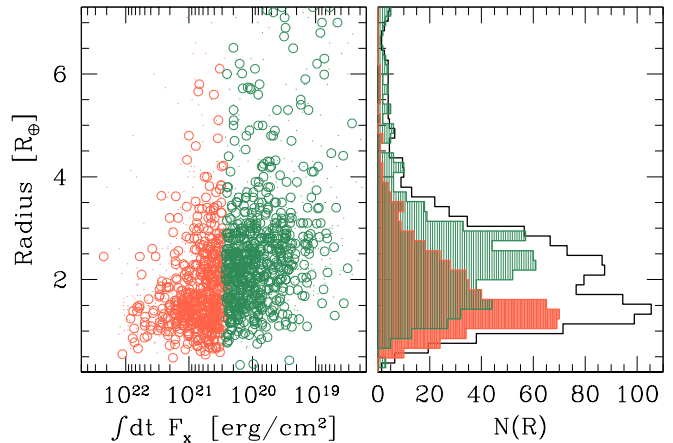


FIG. 9.— The correlation between radii of KOI and their X-ray exposures. In the left panel, we show the radii of KOIs in multi-planet systems (in open circles), and in KOI singles (dots), versus their integrated X-ray exposure. The division between the red and the green population corresponds to a distance of 0.1 AU around a sun-like star. The black solid histogram in the right panel is the size distribution of all KOI multi-planet systems (dashed histogram for singles), while green that of the low X-ray group and red the high X-ray group. The red and green objects have distinctly different peak sizes, as is expected from our X-ray evaporation models (Figure 8). While the green objects (with a peak size at $\sim 2.5R_{\oplus}$) manage to hold on to some of the hydrogen envelopes they were born with, most of the red objects have been stripped down to naked cores (with a peak size at $\sim 1.5R_{\oplus}$). The bimodal size distribution of KOIs is naturally explained by their mass-loss history (see text).

at by Morton & Swift (2013) who construct a probability distribution function rather than using histograms with large ranges. Currently evaporation is the only process that can naturally explain such a bimodality. Any other processes (planet gas accretion, migration, orbital instability, planetary mergers) may lead to a correlation between planet size and location, but will not produce two separate peaks in radius.

The presence of this gap provides strong evidence that evaporation not only sculpts the upper envelope of planet sizes, it is also driving the evolution of the majority of KOI objects. If all the planets in the higher X-ray exposure peak originally had significant H/He envelopes comparable to the planets with lower X-ray exposures, then $\sim 50\%$ of *Kepler* planet candidates having experienced significant mass-loss during their lifetimes. Comparing the gap location (0.1 AU around sun-like star) against our theoretical calculations, we suggest that the planet population in the current KOI list⁶ have predominately low mass cores $\sim 6 M_{\oplus}$, and that most started out their lives with Hydrogen/Helium envelopes of at least a few percent in mass. Certainly, the radius distribution of close-in planets requires further work - along the lines of Morton et al. (2013) - before definitive conclusions can be drawn. As an accurately determined bi-modal distribution encodes value information about the initial and final planet mass and composition. Figure 8 illustrates that the gap radius, as well as the separation at which this gap appears, are direct probes of the core properties. An improved investigation on core composition and

⁶ The apparent absence of bare rocky planets at large separations deserves a comment. The current KOI list is incomplete for this population (Howard et al. 2012; Fressin et al. 2013; Petigura et al. 2013). As such, their presence is not yet understood.

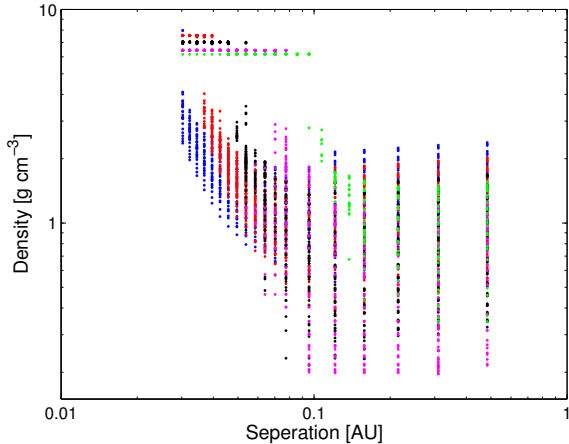


FIG. 10.— Same as Figure 8 but showing final planet density.

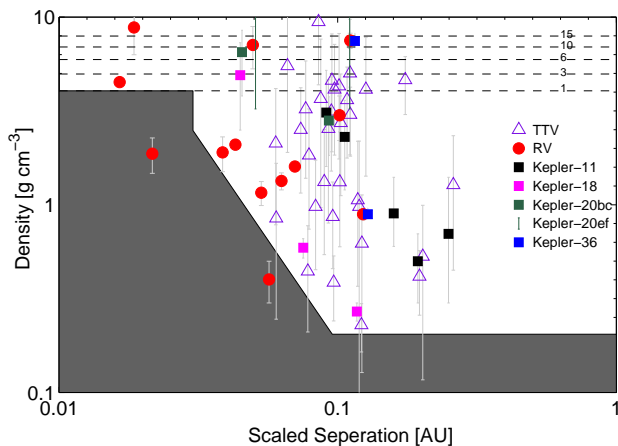


FIG. 11.— Observed planet density plotted against orbital separation, scaled to have the same X-ray exposure as around a sun-type star. The planet sample includes both those from radial velocity surveys (red filled circles, as compiled by Weiss et al. 2013) and Kepler planets with masses confirmed by the *Kepler* team (compiled from Lissauer et al. 2011; Cochran et al. 2011; Gautier et al. 2012; Carter et al. 2012) or calculated from transit timing variations (TTV) by Wu & Lithwick (2013). There are large error bars to many of the TTV masses. The shaded region is the disallowed region as shown in Figure 10, and the dashed lines show the densities of bare rocky cores for a range of masses.

mass should be conducted when planet radii are better determined.

4.3. Comparison of Planet Density

While the KOI catalogue only allows comparison of planet radius, the small but growing sample of low-mass planets with measured masses also provides another important comparison: planet density. In Figure 10, we illustrate planet densities resulting from our integration. In the density-separation plane, the upper envelope in planet size is now translated into a lower envelope in planet density. There is a gap in planet density, similar to that in radius. However, if there is a planet population with low mass cores ($1 - 3M_{\oplus}$), these low density cores may partially fill in the gap.

To compare, in Figure 11 we plot the measured densities of a list of low masses planets against their scaled separations. We scale the actual planet separation by their

respective X-ray exposure, though since most host stars are solar-type, this correction is typically small ($< 10\%$). The theoretically disallowed low-density region is shown. Most of the observed densities avoid this forbidden region, providing strong evidence for sculpting by evaporation.

Current density measurements (especially those using transit-timing fittings) contain large uncertainties. This prevents us from making more quantitative comparisons at the moment. In particular, we could not discern the density gap as predicted by model calculations.

The particular case of Kepler-36bc (Carter et al. 2012) is worth commenting. The two planets have nearly identical separations (0.115 AU and 0.128 AU) but largely discrepant densities, 6.8 & 0.86 g cm^{-3} , respectively. At their present orbits, the minimum core masses for the two planets to retain their envelopes is $\sim 6.5 M_{\oplus}$ (see Figure 10). The measured masses of the two planets are $4.45 M_{\oplus}$ and $8.08 M_{\oplus}$, respectively, naturally explaining the diversity in their structure. More systems like Kepler-36 will be able to provide strong constraints on the nature and strength of evaporation in close-in planetary systems.

5. DISCUSSIONS

We discuss some of the caveats and limitations of the presented calculations and how they bear on our inferences about the observed planet population. The two most important assumptions concern the use of a two-layer planetary model (a rock core plus a Hydrogen/Helium envelope), and the adoption of the Owen & Jackson (2012) evaporation model.

5.1. Variations in the planetary structure

Low-mass planets could contain volatile-rich atmospheres, they could also contain a significant amount of iron and/or ice in their cores, (Adams et al. 2008; Rogers & Seager 2010). Our simple two-layer model of rocky cores plus hydrogen envelope has been successful in explaining the observations. But what about these other possibilities? Can we exclude them based on current observations?

We can exclude the possibility that the dominant primordial atmospheres of these low-mass planets are very rich in volatiles. Our arguments below run similarly to those given in Wu & Lithwick (2013) but are more informed by our detailed modelling and by the physics of evaporation. If one considers a water-rich envelope, for instance, evaporation will not proceed as is described here. First, water molecules have to be photo-dissociated, then oxygen has to settle out to produce a nearly pure hydrogen upper atmosphere (e.g. Kasting & Pollack 1983). If oxygen is present in the evaporative flow at a high enough concentration, it will produce strong cooling and increase the opacity to the X-rays. This will severely suppress the gas temperature, leading to a much lower evaporation rate, similar to what occurs in a high metallicity protoplanetary discs (Ercolano & Clarke 2010), but more extreme. Now suppose all these conditions are satisfied and all hydrogen in the water atmosphere is lost, this removes $1/8$ of the atmosphere mass. However, since the original water atmosphere has a low scale height, such a removal can hardly change either the bulk size or the bulk density of the planet. One

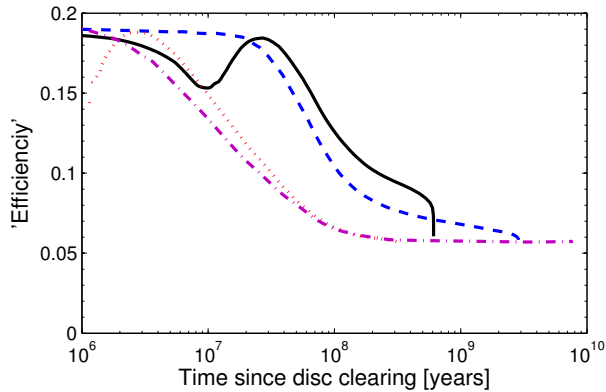


FIG. 12.— The evaporation ‘efficiency’ (η) as a function of time. Here, we trace the evolution of four $20 M_{\oplus}$ planets, with core masses of 7.5 (solid), 10 (dashed), 12.5 (dotted) & 15 (dot-dashed) M_{\oplus} , at a separation of ~ 0.03 AU from a sun-like star. All models lose their entire envelopes towards the end.

would therefore not be able to explain the upper envelope in the observed planet radius, or the bimodal planet size distribution, or the correlation between planet density and X-ray exposure in terms of planetary evaporation.

In contrast to atmosphere composition, we can be less certain about the core composition. For planets with hydrogen envelopes that are more than a percent in mass, the planet sizes are not sensitive to the core sizes (or equivalently, core composition). Planets that have been evaporated down to bare cores may be able to inform us on the core composition, if the core masses are known. A number of these objects show densities that are compatible with rocky or iron/rock compositions (e.g., Hatzes et al. 2011; Batalha et al. 2011). More detailed investigations are necessary to ascertain the core compositions.

5.2. Improving the evaporation model

As we have discussed previously, evaporation is key to the evolution of close in planets. Thus it is important to assess the role the assumed evaporation model plays in our conclusions. Most previous attempts to model the evolution of evaporating planets use a constant evaporation efficiency (η), which is typically taken to be $\sim 10\%$ (e.g., Lopez et al. 2012). We have argued that this efficiency depends on planet mass and radius, as well as on the X-ray flux. We further demonstrate this point here by showing how the efficiency changes as a planet evolves in Figure 12. Following four planets with the same initial mass of $20M_{\oplus}$ (but different core masses), we find that η can decrease by a factor of 4 as the planets evolve from the early puffy stage to the later denser stage, though the variations are not strictly monotonic in time. The overall decrease can be understood: as the planet evolves due to mass-loss and thermal contraction, the planet’s density and the surface escape velocities increases with time. Therefore, it takes longer to accelerate the flow to the escape velocity. This leads to enhanced cooling and lower efficiencies. The non-uniform evolution of some of the models at early times is due to planets straddling the peak efficiency line (roughly when $T_{\text{gas}} \sim T_{\text{escape}}$, see Owen & Jackson 2012) during their evolution and moving above and below it at early times.

While the fixed efficiency of $\sim 10\%$ adopted by, e.g., Jackson et al. (2012); Lopez et al. (2012) does represent

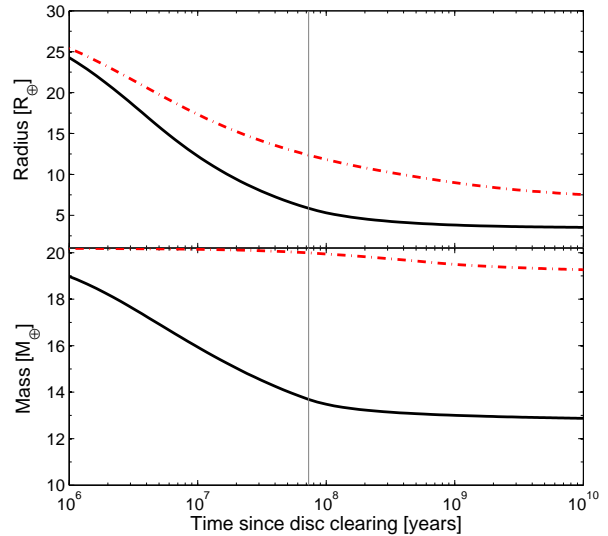


FIG. 13.— The mass and radius evolution of a $20 M_{\oplus}$ planet with a $12.5 M_{\oplus}$ core at a separation of ~ 0.05 AU undergoing standard Owen & Jackson (2012) evaporation (solid) -same as shown in Figure 3- and pure EUV evaporation (dashed). The thin solid line represent the time at which the X-rays/EUV begin to decline.

the approximate median value during the evolution, it can result in order unity inaccuracies in the integrated mass-loss. So any inferences about the initial planet structure should be taken with caution.

5.2.1. Accuracy of the X-ray model

The Owen & Jackson (2012) model for X-ray evaporation contain a number of assumptions that may impact our conclusions here. First, since only the soft $< 1 - 2$ keV photons are responsible for heating, while the X-ray flux refers to the entire observed X-ray spectrum ($0.1 - 10$ KeV). If the adopted X-ray spectrum -while based on observed spectra (see Owen et al. 2010)- is overly soft or overly hard, then the X-ray heating will be over- or under-estimated, respectively. Second, these calculations assumed that, in the X-ray region, molecules are photo-dissociated or thermally dissociated by UV photons. Therefore, Owen & Jackson (2012) neglected cooling associated with molecular species. This is an important assumption which has not been vigorously tested. If instead the molecular species provide significant cooling (in the temperature range of $2000 - 5000\text{K}$), the X-ray driven flow will not reach $T > 5000\text{K}$ and may remain sub-sonic all the way out to the EUV ionization-front. This will markedly reduce the mass-loss rate. More detailed calculations are necessary to address this issue in the future.

5.2.2. The role of EUV Evaporation

We find that EUV evaporation contributes $< 10\%$ of the total mass-loss during the planet’s evolution. The EUV portion of the stellar flux, though comparable in energy to that of the X-rays, are much less efficient at driving a high *integrated* mass-loss. This is because in the EUV flow region, the recombination of hydrogen and the subsequent cooling bleeds much of the energy to space. The radiation hydrodynamics is similar to that of a HII region where ionization is balanced by recombination and

the temperature is controlled by the cooling thermostat to $\sim 10^4$ K (Murray-Clay et al. 2009).

We re-calculate the evolution of our ‘standard’ model (see Section 3.3) undergoing EUV evaporation only, the results of which are shown in Figure 13. At high EUV fluxes ($\gtrsim 10^4$ erg s $^{-1}$), the mass-loss scales as $L_{\text{EUV}}^{1/2}/a$ (Murray-Clay et al. 2009; Owen & Jackson 2012) and is significantly lower than the values that apply to X-ray flow. This suppresses the mass-loss at early times by a factor of ~ 10 , relative to the X-ray model. The integrated mass-loss is $\sim 1 M_{\oplus}$, as opposed to $\sim 7 M_{\oplus}$ in the X-ray model. As such, EUV evaporation alone is unable to sculpt the close-in planet population and cannot explain the observed features discussed in Section 4.

6. CONCLUSIONS

In this work we have coupled the hydrodynamic evaporation models of Owen & Jackson (2012) to the stellar evolution code MESA, in order to follow the mass and radius evolution of low mass planets orbiting close to their stars. Evaporation, while having little effect on massive planets, can remove the entire Hydrogen envelopes for the hottest low-mass planets. In all cases we find that X-rays is the dominant sculpting force, and that most of the mass-loss occurs in the first few 100 Myrs when the stars were more chromospherically active and while the planets were still contracting thermally.

Our main conclusions are as follows:

1. Evaporation produces an upper envelope in planet radius as a function of separation. The location of this upper envelope depends on planet masses and the X-ray luminosity of the host stars. In particular, M-dwarfs, having proportionally larger X-ray fluxes, should have stronger evaporative power than indicated by their low bolometric luminosities.
2. To closely reproduce the observed upper envelope in *Kepler* candidates, both around sun-like stars and around stars of other spectral types, we require that the most massive hot Neptunes should have total masses not much exceeding $\sim 20 M_{\oplus}$, and core masses roughly half of that.
3. Very close-in planets can be stripped of their entire atmosphere. The boundary between complete loss and planets that can retain at least $\sim 1\%$ of their atmosphere lies at ~ 0.1 AU if the core masses are $\sim 6M_{\oplus}$. At this distance (where most of the *Kepler* planets lie), a thinner envelope can not survive. So

we expect a gap in planet size distribution – and this is suggestively seen in the *Kepler* catalogue, where there is a deficit of planets at $\sim 2R_{\oplus}$ straddling planets with high X-ray exposures and those with low X-ray exposures. Comparison with our models suggests that most of the *Kepler* planets should have core masses $\sim 6M_{\oplus}$ and should have primordial Hydrogen/Helium envelopes at least a percent in mass. Moreover, about half of the *Kepler* planets belong to the high X-ray group and have been stripped down to naked cores.

4. Evaporation naturally explains the observed correlation between planet density and separation. At closer separations, planets in general have higher densities.
5. Combining all evidences that support evaporaton, we argue that *Kepler* planets were born with hydrogen envelopes, not volatile-rich atmospheres (also see Wu & Lithwick 2013).

Looking ahead, we expect that the approach we adopt here, coupling thermal evolution and evaporation, will perhaps be the only hope we have for recovering the initial structure of low-mass planets. With better determined stellar radii and hence more accurate planet radii, we may be able to retrieve the initial distribution of planet total masses and core masses. With more measurements of planet densities, it may be possible to reconstruct the histories of individual planets (as is done for *Kepler*-11 by Lopez et al. 2012). A larger sample of planets with measured masses and radii will allow us to place constraints on the core compositions, as well as initial planet entropy. It is at this point that we will begin to learn valuable information about the planet population at birth and make inferences about the planet formation process (e.g Ida & Lin 2005; Mordasini et al. 2012a,b; Hansen & Murray 2012, 2013).

We are grateful to the anonymous referee for comments that helped improve the paper. We thank Norman Murray, Chris Thompson, Jason Rowe, Alan Jackson, Eric Lopez, Adam Burrows and Yoram Lithwick for interesting discussions. The calculations were performed on the Sunnyvale cluster at CITA which is funded by the Canada Foundation for Innovation. YW acknowledges support by NSERC and the Province of Ontario.

REFERENCES

- Adams, E. R., Seager, S., & Elkins-Tanton, L. 2008, *ApJ*, 673, 1160, 1160
- Armitage, P. J. 2011, *ARA&A*, 49, 195, 195
- Baraffe, I., Chabrier, G., & Barman, T. 2008, *A&A*, 482, 315, 315
- Baraffe, I., Selsis, F., Chabrier, G., et al. 2004, *A&A*, 419, L13, L13
- Batalha, N. M., Borucki, W. J., Bryson, S. T., et al. 2011, *ApJ*, 729, 27, 27
- Batalha, N. M., Rowe, J. F., Bryson, S. T., et al. 2013, *ApJS*, 204, 24, 24
- Bertoldi, F., & McKee, C. F. 1990, *ApJ*, 354, 529, 529
- Borucki, W. J., Koch, D. G., Basri, G., et al. 2011, *ApJ*, 736, 19, 19
- Brown, T. M., Latham, D. W., Everett, M. E., & Esquerdo, G. A. 2011, *AJ*, 142, 112, 112
- Carter, J. A., Agol, E., Chaplin, W. J., et al. 2012, *ArXiv e-prints*, arXiv:1206.4718
- Ciardi, D. R., Fabrycky, D. C., Ford, E. B., et al. 2013, *ApJ*, 763, 41, 41
- Cochran, W. D., Fabrycky, D. C., Torres, G., et al. 2011, *ApJS*, 197, 7, 7
- Davis, T. A., & Wheatley, P. J. 2009, *MNRAS*, 396, 1012, 1012
- Erocolano, B., & Clarke, C. J. 2010, *MNRAS*, 402, 2735, 2735
- Erkaev, N. V., Kulikov, Y. N., Lammer, H., et al. 2007, *A&A*, 472, 329, 329
- Fortney, J. J., Marley, M. S., & Barnes, J. W. 2007a, *ApJ*, 668, 1267, 1267

- . 2007b, *ApJ*, 659, 1661, 1661
- Fortney, J. J., & Nettelmann, N. 2010, *Space Sci. Rev.*, 152, 423, 423
- Fressin, F., Torres, G., Charbonneau, D., et al. 2013, *ApJ*, 766, 81, 81
- Gautier, III, T. N., Charbonneau, D., Rowe, J. F., et al. 2012, *ApJ*, 749, 15, 15
- Güdel, M. 2004, *A&A Rev.*, 12, 71, 71
- Güdel, M., Briggs, K. R., Arzner, K., et al. 2007, *A&A*, 468, 353, 353
- Guillot, T. 2010, *A&A*, 520, A27, A27
- Haisch, Jr., K. E., Lada, E. A., & Lada, C. J. 2001, *ApJ*, 553, L153, L153
- Hansen, B., & Murray, N. 2013, *ArXiv e-prints*, arXiv:1301.7431
- Hansen, B. M. S., & Murray, N. 2012, *ApJ*, 751, 158, 158
- Hatzes, A. P., Fridlund, M., Nachmani, G., et al. 2011, *ApJ*, 743, 75, 75
- Hernández, J., Hartmann, L., Megeath, T., et al. 2007, *ApJ*, 662, 1067, 1067
- Hollenbach, D. J., Yorke, H. W., & Johnstone, D. 2000, *Protostars and Planets IV*, 401, 401
- Howard, A. W., Marcy, G. W., Bryson, S. T., et al. 2012, *ApJS*, 201, 15, 15
- Hubbard, W. B., Fortney, J. J., Lunine, J. I., et al. 2001, *ApJ*, 560, 413, 413
- Hubbard, W. B., Hattori, M. F., Burrows, A., & Hubeny, I. 2007a, *ApJ*, 658, L59, L59
- Hubbard, W. B., Hattori, M. F., Burrows, A., Hubeny, I., & Sudarsky, D. 2007b, *??jnlIcarus*, 187, 358, 358
- Ida, S., & Lin, D. N. C. 2005, *ApJ*, 626, 1045, 1045
- Jackson, A. P., Davis, T. A., & Wheatley, P. J. 2012, *MNRAS*, 422, 2024, 2024
- Johnstone, D., Hollenbach, D., & Bally, J. 1998, *ApJ*, 499, 758, 758
- Kasting, J. F., & Pollack, J. B. 1983, *??jnlIcarus*, 53, 479, 479
- Koskinen, T. T., Aylward, A. D., & Miller, S. 2007, *Nature*, 450, 845, 845
- Koskinen, T. T., Cho, J. Y.-K., Achilleos, N., & Aylward, A. D. 2010, *ApJ*, 722, 178, 178
- Lammer, H., Erkaev, N. V., Odert, P., et al. 2013, *MNRAS*, 664, 664
- Lammer, H., Selsis, F., Ribas, I., et al. 2003, *ApJ*, 598, L121, L121
- Lecavelier des Etangs, A. 2007, *A&A*, 461, 1185, 1185
- Lissauer, J. J., Ragozzine, D., Fabrycky, D. C., et al. 2011, *ApJS*, 197, 8, 8
- Lissauer, J. J., Marcy, G. W., Rowe, J. F., et al. 2012, *ApJ*, 750, 112, 112
- Lopez, E. D., Fortney, J. J., & Miller, N. 2012, *ApJ*, 761, 59, 59
- Mann, A. W., Gaidos, E., Lépine, S., & Hilton, E. J. 2012, *ApJ*, 753, 90, 90
- Mordasini, C., Alibert, Y., Georgy, C., et al. 2012a, *A&A*, 547, A112, A112
- Mordasini, C., Alibert, Y., Klahr, H., & Henning, T. 2012b, *A&A*, 547, A111, A111
- Morton, T. D., & Johnson, J. A. 2011, *ApJ*, 738, 170, 170
- Morton, T. D., & Swift, J. J. 2013, *ArXiv e-prints*, arXiv:1303.3013
- Muirhead, P. S., Hamren, K., Schlawin, E., et al. 2012, *ApJ*, 750, L37, L37
- Murray-Clay, R. A., Chiang, E. I., & Murray, N. 2009, *ApJ*, 693, 23, 23
- Nettelmann, N., Fortney, J. J., Kramm, U., & Redmer, R. 2011, *ApJ*, 733, 2, 2
- Owen, J. E., Ercolano, B., & Clarke, C. J. 2011, *MNRAS*, 412, 13, 13
- Owen, J. E., Ercolano, B., Clarke, C. J., & Alexander, R. D. 2010, *MNRAS*, 401, 1415, 1415
- Owen, J. E., & Jackson, A. P. 2012, *MNRAS*, 425, 2931, 2931
- Paxton, B., Bildsten, L., Dotter, A., et al. 2011, *ApJS*, 192, 3, 3
- Paxton, B., Cantiello, M., Arras, P., et al. 2013, *ArXiv e-prints*, arXiv:1301.0319
- Perez-Becker, D., & Chiang, E. 2013, *ArXiv e-prints*, arXiv:1302.2147
- Petigura, E. A., Marcy, G. W., & Howard, A. W. 2013, *ArXiv e-prints*, arXiv:1304.0460
- Ribas, I., Guinan, E. F., Güdel, M., & Audard, M. 2005, *ApJ*, 622, 680, 680
- Rogers, L. A., & Seager, S. 2010, *ApJ*, 712, 974, 974
- Tian, F., Toon, O. B., Pavlov, A. A., & De Sterck, H. 2005, *ApJ*, 621, 1049, 1049
- Vidal-Madjar, A., Lecavelier des Etangs, A., Désert, J., et al. 2003, *Nature*, 422, 143, 143
- Vidal-Madjar, A., Désert, J.-M., Lecavelier des Etangs, A., et al. 2004, *ApJ*, 604, L69, L69
- Watson, A. J., Donahue, T. M., & Walker, J. C. G. 1981, *Icarus*, 48, 150, 150
- Weiss et al. 2013, *ArXiv e-prints*, arXiv:1303.2150
- Wu, Y., & Lithwick, Y. 2013, *ArXiv e-prints*, arXiv:1210.7810
- Yelle, R. V. 2004, *Icarus*, 170, 167, 167